

# Studies of the UHECR propagation in the Galactic Magnetic Field

S. Vorobiov<sup>a</sup>, M. Hussain<sup>a</sup>, and D. Veberič<sup>ab</sup>

<sup>a</sup>Laboratory for astroparticle physics, University of Nova Gorica, Slovenia

<sup>b</sup>J. Stefan Institute, Ljubljana, Slovenia

We present the results of simulations of the ultra-high energy cosmic ray (UHECR) propagation in the Galactic magnetic field (GMF). Different assumptions on the large-scale GMF structure and/or primary particle lead to distinctly different deflection patterns of the highest energy cosmic rays (CR). The GMF modifies the exposure of an UHECR experiment to the extragalactic sky. We estimated these effects for the Pierre Auger experiment. Further forward-tracking studies under plausible UHECR sources scenarios will allow for direct comparison with the observed correlation between the nearby active galactic nuclei (AGN) and the highest energy Auger events.

## 1. Introduction

Magnetic fields in the Milky Way are investigated via Faraday rotation of the polarized light from pulsars and extragalactic (EG) sources, and through measurements of the Galactic synchrotron radiation [1,2]. The observations reveal the presence of a large-scale (LS) Galactic magnetic field (GMF), that in the first approximation follows the spiral arm structure. The LS field extends above and below the Galactic disk on a kiloparsec scale and forms a kind of halo. A random GMF, of the strength similar to that of the regular component, but with the coherence length of only  $\sim 50$  pc, has also been observed [1]. The average strength of the total magnetic field near the Sun is about  $6 \mu\text{G}$ . However, details of the field distribution are poorly known [3,4,5].

The Pierre Auger Observatory [6] provides a new and independent way of studying cosmic magnetic fields, by collecting CR events above  $10 \text{ EeV} \equiv 10^{19} \text{ eV}$  with unprecedented statistics and data quality. Recently, Auger observed a significant correlation (over angular scales  $\leq 6^\circ$ ) of the arrival directions of CR above  $\simeq 60 \text{ EeV}$  with the locations of nearby AGN [7,8], and a strong steepening of the CR flux above  $40 \text{ EeV}$  [9]. Both observations are consistent with the standard UHECR astrophysical acceleration scenarios and thus represent an important step towards the “charged particle astronomy”.

The elaboration of relevant analysis methods for the UHECR astronomy requires detailed investigation of the cosmic ray propagation in the GMF. We present in this paper results of such studies, performed in the light of the observed AGN correlation. We used the standard method of CR backtracking. A large number of CR events has been simulated using parameters described below, and propagated under three distinctive large-scale GMF models. We present the resulting magnetic deflections and modification of the extragalactic exposure due to the LS GMF.

## 2. Implementation of CR backtracking

To obtain the UHECR trajectories, we implemented the integration of the equations of motion of an ultrarelativistic particle in the magnetic field using the Runge-Kutta 5<sup>th</sup> order scheme with the adaptive step size control [10]. The particles have been followed till the galactocentric distance of  $20 \text{ kpc}$  (the Galaxy “border”), beyond which the GMF strength is supposed to be negligibly small. An accuracy level (the accepted truncation error) of  $10^{-6}$  has been adopted, for which the changes in the backtracked directions become negligible with respect to the chosen step in angular separation  $d_{\text{max}}$  from the selected astrophysical objects (see the section 6.1). To avoid the “numerical dissipation” of the CR energy [11], we preserved the absolute value of the CR velocity vector during propagation.

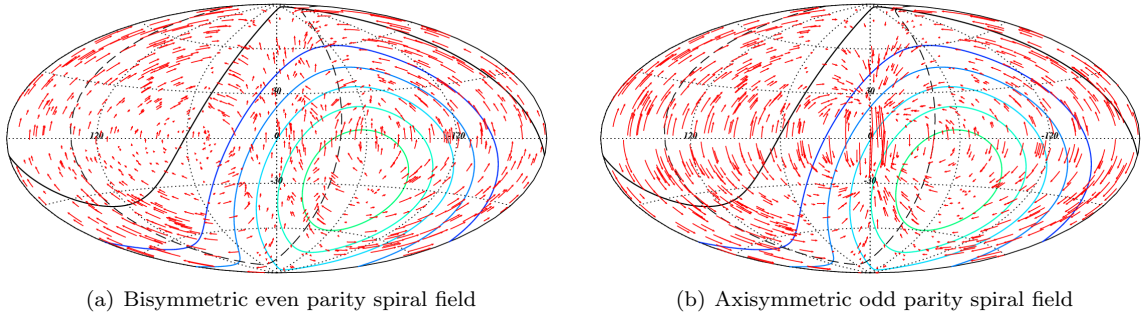


Figure 1. Cosmic ray deflection patterns for *protons* under Models I and II. Arcs of great circles join the simulated arrival directions on Earth, and the backtracked ones at the Galaxy border (arrow heads). Every 1000<sup>th</sup> event is shown. The dashed line denotes the supergalactic plane (SGP). The solid lines show the equal integrated Auger SD exposure sky regions within the detector field of view for  $\theta_z \leq 60^\circ$ .

### 3. Parameters of simulated CR events

**Energies** of the simulated events were bounded between 40 EeV and 150 EeV, and distributed according to the Auger measurement [9], as a power law  $E^{-4.2}$ .

Two options for the **angular distribution** of the events have been considered: 1) Uniform over the whole sky ( $10^6$  events), and 2) According to the exposure of the Auger Surface Detector (SD) for zenith angles  $\theta_z \leq 60^\circ$  [12,13] ( $10^5$  events).

Four pure **mass compositions** have been considered: protons, carbon, silicon, and iron nuclei.

### 4. Considered large-scale GMF models

We have chosen amongst many available large-scale GMF models *three* typical ones with distinct qualitative differences. Two models are the spiral disk field models of *bisymmetric even parity* (hereafter **Model I**), and *axisymmetric odd parity* (**Model II**) from the paper [14] by Harari, Mollerach and Roulet (HMR).

**Model III** is a modification of the model [15] by Prouza and Šmída (PS), that has been proposed by Kachelrieß *et al.* [16]. In addition to the *bisymmetric even parity* spiral field, of the structure similar to the one in Model I, it features two additional large-scale halo GMF components: *toroidal* azimuthal field above and below

the Galactic disk, and *poloidal* (dipole) field.

### 5. Magnetic deflections of cosmic rays

The cosmic ray deflection patterns obtained using the three selected GMF models are very different, and have trends, typical for each model. Fig. 1 shows deflections of primary *protons* for Models I and II. In the bisymmetric even parity field, CR arrival directions at the Galactic border point in general to higher Galactic latitudes than observed on Earth. In the odd parity field, the backtracked arrival directions in each Galactic hemisphere are shifted to the poles, and no cosmic rays are coming from the directions close to the Galactic plane. The presence of dipole and toroidal fields in Model III makes the deflection pattern even more complex [17].

The deflection values for the three GMF models, and *the Auger SD exposure* are summarized in the table 1, by means of percentiles at 50% (median), and 95.45% of the c.d.f. The median deflection values scale well with the atomic number  $Z$  of primary nuclei. They are larger for the HMR models than in Model III, due to the more important halo field extension.

The simulated events allow to roughly estimate the corresponding deflections expected from turbulent magnetic fields [17]. Compared to the deflections from the large-scale field, the former ones

have to be much smaller, which is confirmed by simulations including turbulent field [18], and can be neglected at the first approach.

## 6. GMF effects on the EG exposure

(De-)focusing effects of the Galactic magnetic field make the correspondence between the CR arrival directions on Earth, and the EG sources contributing to the CR flux entering the Galaxy non-trivial [14,16,19]. We have constructed maps of parameter  $\Lambda \equiv \log_{10}$  of the ratio of the number of CR arrivals on the halo border to the one on Earth, using the HEALPix equal area celestial sphere pixelization [20]. These maps are shown on Fig. 2 for the case of primary *carbon* nuclei.

Due to these effects, some regions of the sky have increased probability to contribute to the cosmic rays observed on Earth, and some others are disfavored. The non-uniform character of the mapping strengthens in the case of heavy composition [17], so that the regions that would effectively contribute to the CR flux on Earth represent only a small fraction of the  $4\pi$  solid angle.

### 6.1. Correlation scan using backtracked directions

To quantify the lensing GMF effects on the EG exposure for the Pierre Auger Observatory, we performed a correlation analysis using *backtracked* arrival directions of simulated events, and 694 AGN at redshift  $z_{\max} \leq 0.024$  from the VCV catalogue [21]. The simulated CR have been divided sequentially into samples with the same number of events (81) above 40 EeV as in the Auger data. The employed set and ranges of parameters were also identical to the ones from [7,8].

We will focus here on the minimum probability values, obtained during the scan. The c.d.f. of decimal logarithm of the corresponding cumulative binomial probability  $P_{\min}$  of reaching this level of correlation under isotropy for Model I are shown on Fig. 3. The level of the minimum probability reached in the Auger data is also indicated. The results of the correlation scan for the assumed LS GMF models and primary mass compositions are summarized in Table 1.

Since for the different GMF model/primary

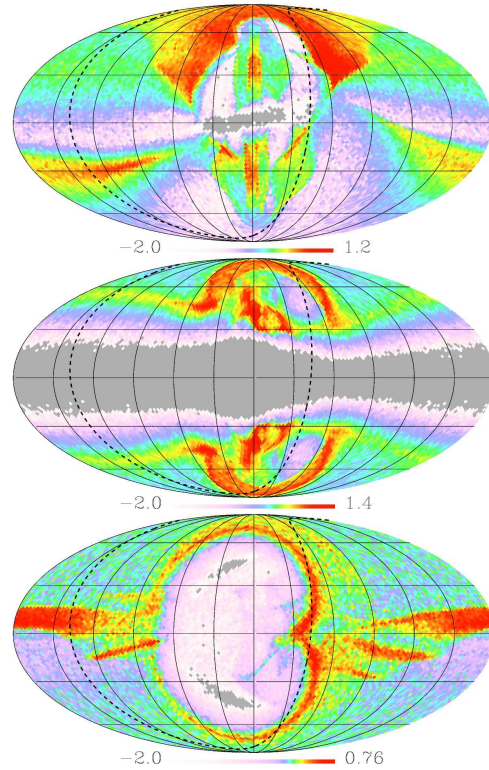


Figure 2. Sky maps of the  $\Lambda$  values for Models I (upper), II, and III (lower), and *carbon* nuclei. Earth UHECR detectors are (almost) blind to the regions in gray. The dashed line denotes the SGP.

mass assumptions the backtracked directions correlate with the catalogue objects in particular privileged regions in the sky, our scan results depend strongly on those assumptions. For Model III, the scanned probability minimum is significantly less deep than for the two other spiral-field-only models for any assumed primary mass, except for protons, where one obtains nearly the same level of correlation for all models. This model is clearly less compatible with the observed correlation with the nearby AGN [7,8], unless the UHECR flux contribution from these objects (or objects with similar spatial distribution) is highly non-uniform.

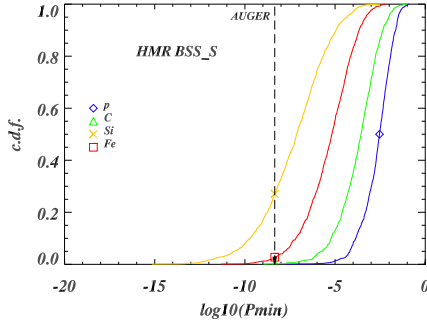


Figure 3. Scan results (c.d.f. of  $\log_{10} P_{\min}$ ) of the simulated CR samples, backtracked under Model I and 4 masses. The dashed line shows the value from the Auger scan [7,8] on Earth. C.d.f. for protons (shown by symbol at the median value) does not intersect this line.

	Deflections		Scan results		
	$\vartheta_{50\%}$	$\vartheta_{95.45\%}$	$f_{5\%}$	$f_{50\%}$	$f_{95\%}$
<b>HMR bisymmetric even parity model</b>					
p	4.1	7.4	-4.2	-2.5	-1.5
C	23.7	53.4	-5.8	-3.6	-2.0
Si	52.3	117.3	-10.6	-7.1	-4.3
Fe	74.5	162.4	-7.8	-5.2	-3.3
<b>HMR axisymmetric odd parity model</b>					
p	4.3	10.3	-4.5	-2.6	-1.6
C	25.5	84.1	-8.9	-5.8	-3.7
Si	65.0	141.8	-12.6	-8.7	-5.5
Fe	81.1	146.3	-9.6	-6.3	-4.0
<b>PS model version by Kachelrieß <i>et al.</i></b>					
p	3.0	30.1	-4.2	-2.5	-1.5
C	17.6	76.2	-4.3	-2.5	-1.4
Si	37.4	92.0	-4.9	-3.0	-1.7
Fe	58.3	124.7	-4.2	-2.6	-1.5

Table 1

Magnetic deflections (in  $^\circ$ ), and  $\log_{10} P_{\min}$  values at the indicated percentiles of the c.d.f., for the assumed GMF models and primary mass.

## 7. Conclusions and outlook

Our studies of the UHECR propagation in the LS GMF show that the UHECR picture observed on Earth is sensitive to the assumptions on the field structure and/or primary CR composition.

The exact deflection value in the regular component of the field depends strongly on the arrival direction on Earth of a cosmic ray, with the corresponding position angle of deflection differing from one assumed field distribution to another. To discriminate between GMF models, additional hints can be provided by the aligned structures of events coming from a UHECR source [22].

Though the reconstruction of the field is easier in the case of light primary mass composition, in the case of heavy nuclei the lensing effects of the Galactic field on the exposure bring stronger constraints on the list of potential UHECR source candidates. The presented analysis of the correspondence between the arrival direction distributions on Earth and at the Galactic border will be complemented by the forward-tracking of cosmic rays for a number of plausible UHECR sources scenarios. This will allow for direct comparison with the observed AGN correlation.

## REFERENCES

1. R. Beck, Space Sci. Rev., **99** (2001) 243, astro-ph/0012402.
2. L. M. Widrow, RMP **74** (2002) 775, astro-ph/0207240.
3. J. L. Han *et al.*, ApJ **642** (2006) 868, astro-ph/0601357.
4. J. C. Brown *et al.*, ApJ **663** (2007) 258, arXiv:0704.0458.
5. H. Men *et al.*, A&A **486** (2008) 819, arXiv:0805.3454.
6. <http://www.auger.org>.
7. J. Abraham *et al.*, Science **318** (2007) 939, arXiv:0711.2256.
8. J. Abraham *et al.*, APh **29** (2008) 188, arXiv:0712.2843.
9. J. Abraham *et al.*, PRL 101 (2008) 061101, arXiv:0806.4302.
10. W. H. Press *et al.*, ISBN 0-521-43108-5.
11. E. Armengaud, PhD, Univ. Paris 7 (2006).

12. P. Sommers, *Astropart. Phys.* **14** (2001) 271, astro-ph/0004016.
13. D. Allard for the Pierre Auger Collaboration, Proc. 29<sup>th</sup> ICRC, paper no. 134, astro-ph/0511104.
14. D. Harari *et al.*, *JHEP* **08** (1999) 022, astro-ph/9906309.
15. M. Prouza and R. Šmída, *A&A* **410** (2003) 1, astro-ph/0307165.
16. M. Kachelrieß *et al.*, *APh* **26** (2006) 378, astro-ph/0510444.
17. S. Vorobiov *et al.*, 2009, arXiv:0901.1579.
18. P. Tinyakov, I. Tkachev, *APh* **24** (2005) 32, astro-ph/0411669.
19. J. Alvarez-Muñiz *et al.*, *ApJ* **572** (2002) 185, astro-ph/0112227.
20. K. M. Górski *et al.*, *ApJ* **622** (2005) 759, astro-ph/0409513.
21. M.-P. Véron, P. Véron, *A&A* **455** (2006) 773.
22. D. Harari *et al.*, *JHEP* **0207** (2002) 006, astro-ph/0205484.